PROCEEDINGS OF SPIE

SPIEDigitalLibrary.org/conference-proceedings-of-spie

Optoacoustic monitoring of RF ablation lesion progression

Francisco Javier Oyaga Landa, Cagla Özsoy, Xosé Luis Deán-Ben, Daniel Razansky

Francisco Javier Oyaga Landa, Cagla Özsoy, Xosé Luis Deán-Ben, Daniel Razansky, "Optoacoustic monitoring of RF ablation lesion progression," Proc. SPIE 10878, Photons Plus Ultrasound: Imaging and Sensing 2019, 108782R (27 February 2019); doi: 10.1117/12.2510775



Event: SPIE BiOS, 2019, San Francisco, California, United States

Optoacoustic monitoring of RF ablation lesion progression

Francisco Javier Oyaga Landa, 1,2 Cagla Ozsoy, 1,3 Xosé Luís Deán-Ben, 1 and Daniel Razansky $^{1,3,\,*}$

¹Institute for Biological and Medical Imaging (IBMI), Helmholtz Zentrum München, Neuherberg, Germany

²Faculty of Informatics, Technical University of Munich, Munich, Germany ³School of Medicine, Technische Universität München (TUM), Munich, Germany *Corresponding author: dr@tum.de

ABSTRACT

Efficient monitoring of radiofrequency ablation procedures is essential to optimize the lesions induced to treat cancer, cardiac arrhythmias and other conditions. Recently, optoacoustic imaging and sensing methods have been suggested as a promising approach to address this challenge, offering unique advantages such as high sensitivity to temperature changes and chemical transformations in coagulated tissues, real-time operation and use of non-ionizing radiation. However, assessing how the ablation lesion boundary progresses is still challenged by changes in optical properties induced during the interventions. Herein, we suggest a new approach for dimensional characterization of the induced lesion based on detecting sharp positive variations in the time derivative of optoacoustic signals. Experiments in porcine tissue samples indicate that such variations are uniquely associated to the onset of ablation and that the method can robustly visualize the evolution of the lesion in three dimensions.

Keywords: Radiofrequency Ablation of Tissue; Optoacoustic Tomography; Temperature; Thermal Treatments.

1. INTRODUCTION

Thermal treatments are routinely used in the clinics for a myriad of applications ranging from pain relief to the generation of localized apoptosis and coagulative necrosis in tumors.¹ The induced thermal effects in biological tissues mainly depend on the temperature rise. No permanent tissue damage is generally produced for temperatures below 50°C, and treatments are typically based on bio-stimulation of chemical reactions in muscle, nervous and other tissues.² At higher temperatures, irreversible effects such as coagulation, carbonization or vaporization of tissues are produced.^{3–5} These effects are exploited for tissue ablation, a term used in medicine to refer to the destruction or removal of diseased (pathological) tissues.⁶ Thermal ablation, performed by either heating or cooling to reach temperatures lethal to cells, is used world-wide with the aim to treat cancer, cardiac arrhythmias and other conditions.⁷ Multiple energy sources such as laser, microwaves, ultrasound and radiofrequency (RF) current can be used for heating,⁸ while cryoablation is performed by circulating fluids through hollow needles (cryoprobes) to reach temperatures typically below -50°C.⁹

Efficient monitoring of ablation procedures is essential for improving the treatment outcome as well as to avoid unnecessary tissue damage.¹⁰ Generally, this is achieved by mapping the spatio-temporal distribution of temperature within the treated region either by inserting sensors at specific locations or with non-invasive imaging modalities such as infrared thermometry, x-ray computed tomography, magnetic resonance imaging or ultrasound.¹¹ Recently, several groups have suggested optoacoustic (OA, photoacoustic) imaging and sensing systems as a new approach for real-time monitoring of tissue ablation with high contrast and by using only non-ionizing excitation.^{12,13} OA presents unique advantages for this purpose as 1) the thermo-elastic conversion efficiency is highly sensitive to temperature variations (2.7% per °C)^{14–18} and 2) tissue coagulation leads to chemical changes further affecting the OA signal intensity.¹⁹ These two effects are clearly evinced in experiments performed for calibrating the temperature dependence of OA signals. It was shown that the increase in OA signal intensity per °C remains approximately constant for temperatures below 50°C, where it abruptly changes.²⁰ This additional increase in OA signal intensity, associated to coagulation of tissues at higher temperatures, was also shown to be maintained when the tissue was cooled down to room temperature. To this end, OA measurements

Photons Plus Ultrasound: Imaging and Sensing 2019, edited by Alexander A. Oraevsky, Lihong V. Wang, Proc. of SPIE Vol. 10878, 108782R \cdot © 2019 SPIE \cdot CCC code: 1605-7422/19/\$18 \cdot doi: 10.1117/12.2510775

performed during thermal ablation procedures have corroborated this initial calibration experiments. Real-time temperature mapping was achieved for temperatures below coagulation thresholds¹⁴ and the ablated region could be identified after cooling down via multi-spectral analysis or comparison with the corresponding image before ablation.²¹ Real-time monitoring further enabled visualizing tissue destruction e.g. in endovenous laser ablation.²² However, assessing how the ablation lesion boundary progresses during an intervention remains challenging. It is known that the resulting lesion size depends both on temperature and exposure time,²³ and OA temperature readings are inaccurate when ablation is produced.²⁴ Tissue coagulation further leads to a change in optical attenuation,²⁵ which in turn produces distortion (spectral coloring) of the absorption spectrum at deep locations. Herein, we suggest a new approach for characterizing the evolution of the induced lesion based on identifying sharp changes in OA time profiles extracted from the sequence of images acquired with a four dimensional (real-time three dimensional) OA tomographic imaging system. The method is based on single-wavelength excitation and hence is not affected by spectral coloring or other OA signals changes in the optical wavelength dimension.

2. METHODS/RESULTS

A lay-out of the experimental set-up is depicted in Fig. 1a. Radiofrequency (RF) ablation was induced on a 30x30x10mm³ porcine heart tissue sample using a RF wave generator and an electrode with a 3 mm diameter semi-spherical shaped tip. A second (ground) electrode consisting of an aluminum foil was placed at the bottom surface of the tissue. The RF generator delivered bursts of 600 cycles at 20 kHz (Fig. 1b) with an average power of 9 W. Volumetric (three-dimensional - 3D) OA imaging was performed with a self-developed tomographic imaging system consisting of a 512-element spherically-arranged transducer array covering an angle of 140° (1.3 π solid angle) with 4 cm of curvature radius. Each array element has a central frequency of 5 MHz and 100% detection bandwidth, which enables a nearly isotropic resolution of $150 \mu m$ around the geometrical center of the spherical array. 11 Efficient acoustic coupling and electrical insulation were facilitated by an agarose layer positioned between the active surface of the imaging array and the electrical ground pad. OA excitation was provided with a 10 Hz short-pulsed (¡10 ns) laser (Innolas Laser GmbH, Krailling, Germany) guided via a custom-made fiber bundle (CeramOptec GmbH, Bonn, Germany) through a central cavity in the array. The laser wavelength was set to 780 nm to provide maximum contrast between ablated and non-ablated tissues. 21 The energy density per pulse and mean power density of the light beam at the tissue surface were maintained below safety standards.²⁶ A custom-made data acquisition system (DAQ, Falkenstein Mikrosysteme GmbH, Taufkirchen, Germany) was used for simultaneous acquisition of all 512 pressure signals at 40 megasamples per second. The acquired pressure signals were deconvolved with the frequency response of the array elements and band-pass filtered between 0.1 and 4 MHz. 3D OA images were subsequently reconstructed with a graphics processing unit (GPU)-based 3D back-projection algorithm.⁹

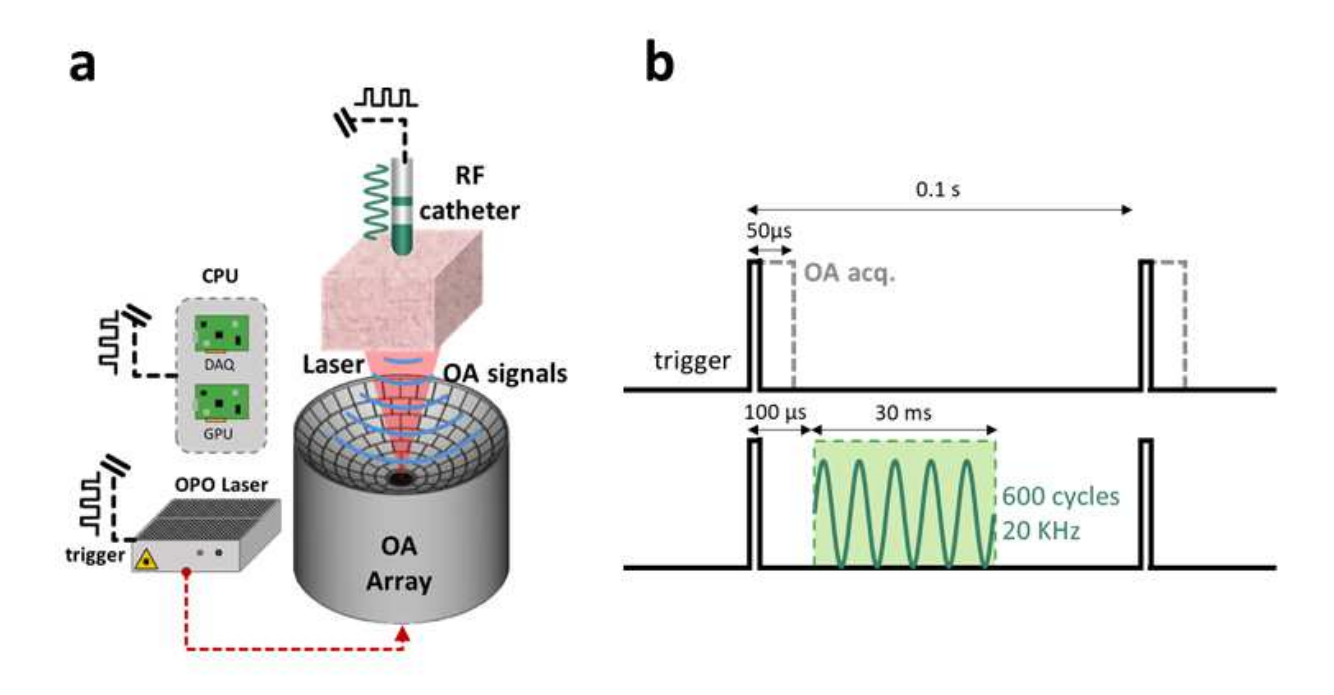


Figure 1. Schematic view of the experimental setup of the ablation experiment. (a) Drawings of the OA transducer array and RF system network. (b) Schematic synchronization diagram of the OA and RF excitations and acquisition routines.

For short-pulsed laser excitation under thermal and stress-confinement conditions,²⁷ the OA signal (initial pressure) is approximately given by $p_0 = \Gamma \mu_a \phi$, being Γ the (dimensionless) Grüneisen parameter, μ_a the optical absorption coefficient and ϕ the light fluence. The Grüneisen parameter is known to be temperature dependent and hence changes in OA signal amplitude can be used to estimate corresponding changes in temperature. Thus, for water and diluted aqueous solutions, the temperature rise at a given point can be estimated from the relative increase in OA signal intensity as²⁸

$$\Delta T = \frac{\Delta P_0(0.8113 + T_0)}{p_{0,0}} \tag{1}$$

being $p_{0,0}$ and T_0 the initial (baseline) OA signal and the initial temperature in 0,0, respectively. DT in Eq. 1 is expressed in °C.

RF ablation was performed in a porcine tissue sample with approximately 1 cm thickness.

The RF catheter containing the electrical excitation is in orthogonal position relative to the surface of the tissue sample. Thermal coagulation is initiated when the tissue resistance to the electrical input leads to a joule-effect temperature increase above the tissue-specific temperature and time of exposure time for tissue denaturation. The procedure is monitored in real-time by illuminating the region of interest treated beneath the electrode. The guiding fiber bundle delivers approximately 20 mJ of electromagnetic radiation and it gets diffused and scattered at the surface of the sample, subsequently leading to an exponential fluence decay in the direction of the beam path. Fig. 2a displays the time profiles of the relative increase in OA signal intensity during ablation for two points located at 6 mm (blue curve) and 10 mm (red curve) depth. Considering that soft biological tissues mainly consist of water, Eq. 1 can be taken as a reasonable approximation. Eq. 1 establishes that the increase in temperature is proportional to the relative increase in OA signal. Thereby, the estimated time profiles of temperature are equivalent to those shown in Fig. 2a for temperatures below the ablation temperature threshold (typically 50°C). However, this approximation is no longer valid when ablation takes place as additional changes in the Grneisen parameter are produced. The time points when the ablation temperature threshold is reached (marked in Fig. 2b) can be identified in the differential profiles of temperature. Such time points can be used to

build a map corresponding to the onset time of ablation that serves to estimate how the lesion propagates with time.

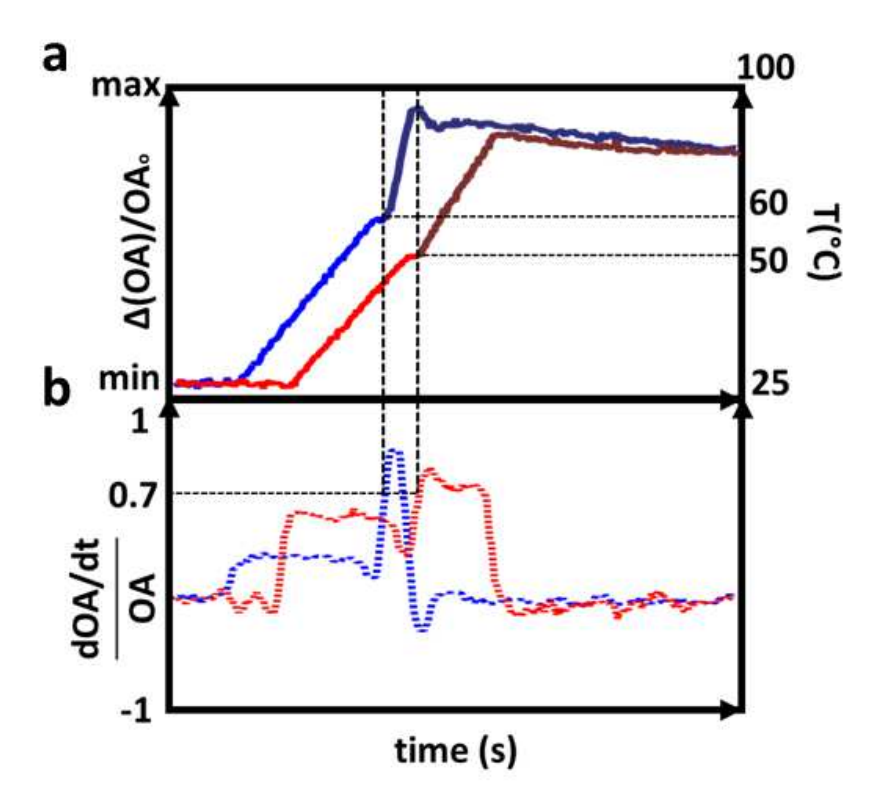


Figure 2. (a) Lay-out of the experimental setup. The RF catheter containing the electrical excitation is positioned orthogonally to the surface of the tissue sample. (b) Computational methods for estimation of the lesion size during RF ablation. OA signal derivative approach and coagulation temperature methods.

The time profile of OA signal intensity in Fig. 2b further features a significant slope change at approximately the time point when the ablation temperature threshold is reached. The below panel in Fig 2b displays the numerically estimated time derivative of the OA signal intensity $(\delta p_0/\delta t)$. Four different intervals can be clearly distinguished. In the first (baseline) interval, $\delta p_0/\delta t = 0$. $\delta p_0/\delta t$ subsequently reaches defined positive values in a second and third intervals, whiles it eventually becomes slightly negative in the final interval. The significant change in $\delta p_0/\delta t$ between the second and third interval is consistent with the previously reported change in slope of the OA signal intensity versus pressure when ablation is produced, ¹⁷ i.e., ablation begins between the second and third intervals in the $\delta p_0/\delta t$ curves. A map of the onset time of ablation can then be estimated from the time points between the second and third intervals by setting a threshold in $\delta p_0/\delta t$ for the voxels in the image. It is also important to note that the relative increase in OA signal for the first point features a relatively sharp decrease at the beginning of the fourth interval. This is arguably due to the fact that the light fluence is reduced when ablation at deeper regions (e.g. at point 2) starts to be produced. Indeed, the onset of ablation leads to an increased optical attenuation and a consequent decrease in light fluence and optoacoustic signal in the entire volume. Thereby, a sharp increase in optoacoustic signal is only produced for the time points when ablation starts, and the identification of these points represents a robust approach for assessing the progression of the lesion being formed.

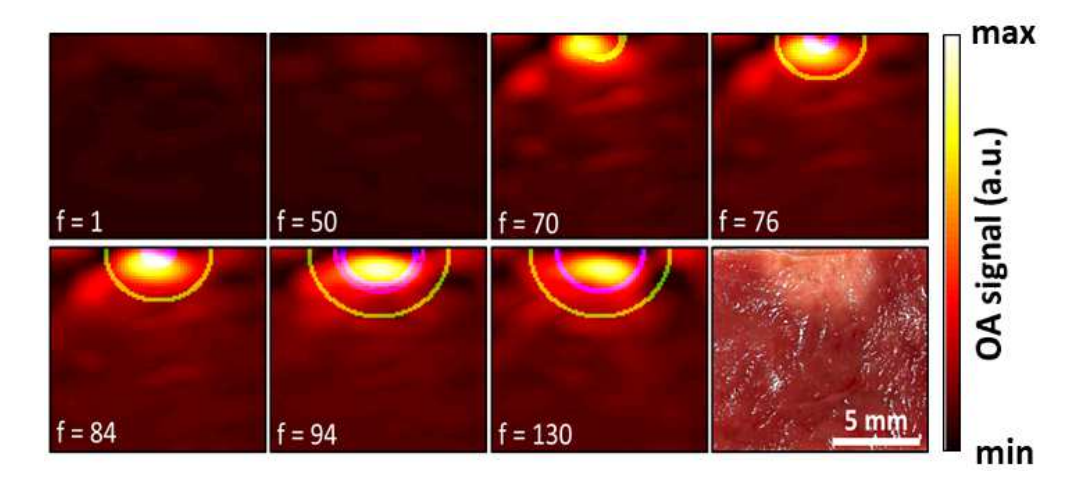


Figure 3. Lesion boundary progression results applying different detection methods. Coagulated region dimensions for width (w) and depth (d) of the ablated tissue displayed with continuous and dashed lines respectively. The coagulation boundary regions overlayed on top of the actual fluence-corrected OA images at different time-points during the treatment and the post-ablation cross-sectional view of the porcine tissue sample.

The lesion width and depth were examined for characterization of the lesion growth as a function of time. The ablated points were identified as those that 1) exceeded a give temperature threshold as estimated optoacoustically or 2) underwent a change in slope in the optoacoustic time profile. Fig. 3 shows the results of this characterization. Fig. 3a displays the measured width (w) and depth (d) of the lesion for two different values of the temperature threshold and for which the derivative of the optoacoustic normalized signal derivative increased by 70%, based on previous studies. 17 It is shown that the lesion size estimated from the derivative of the optoacoustic signal approximately matches that estimated with a temperature threshold of 60°C. This is expected considering that for this temperature coagulation is almost instantaneous and the heating process is rather fast, i.e., a temperature of 60°C is reached before the time required for tissue ablation at lower temperatures, i.e.: 50°C. The dynamics of lesion formation is also visualized in a sequence of maximum intensity projections (MIPs) of the OA images along the lateral plane shown in Fig. 3b. For better visualization, the images were normalized with the light fluence distribution estimated from the diffusion equation for a semi-infinite medium, namely an exponential decay with depth from the illuminated surface with effective attenuation coefficient eff = 3.5 cm^{-1} . A movie of the lesion formation process is provided as supplementary material in the online version of the journal. The dimensions of the lesion estimated with the time derivative of the OA signals (w=6.1 mm and d=2.6 mm) approximately matched the observed lesions size in a photograph of a tissue section taken after the ablation procedure (Fig. 3b), which corroborates the validity of this approach.

3. DISCUSSION

The final size of the ablation lesion estimated both by considering the threshold temperature and the time derivative of the OA signals reasonable agreed with that observed visually in a section of the sample taken after the procedure. This, along with the fact that the results obtained with these two independent methods matched for different time points, appears to ratify the feasibility of OA monitoring of lesion progression in RF ablation procedures. Both methods are based on simple operations that can easily be computed in real-time, which ensures their applicability in the clinical setting.

In principle, the suggested methodology can as well be applied for monitoring the lesion progression in other ablation interventions based on alternative sources of energy. However, this needs to be verified for each specific case. Of particular importance is the induced spatio-temporal distribution of the temperature field. It is well-known that both the temperature and the exposure time have an influence on the resulting ablation lesion in the target tissue. Indeed, it has been noted that for each temperature exposure degree increase above 43°C, there is a two-fold drop in the time required to achieve the same biological denaturation effect.²³ Thereby, some methods to estimate tissue degradation account for both exposure time and temperature. For example, the cumulative

equivalent minutes (CEM) methodology establishes the time required to produce ablation in a tissue exposed to a given temperature.²⁹ These methods can potentially be implemented in the OA framework described in this work. However, accurate estimation e.g. of the CEM at a given point requires the development of more sophisticated models that properly account for the temperature dependence of the OA signals when ablation is produced. Cumulative exposure has a limited effect for the ablation method considered in this work since tissue ablation is produced in relatively short time, but it can be very important in slower procedures. It is also important to take into account that significant changes in the optical properties of tissues are produced when coagulation takes place. This in turn affects the light attenuation in tissues and leads to additional inaccuracies in the estimated temperature maps.

The newly suggested approach based on analyzing the changes in the temporal derivative of the OA signals does not rely on temperature estimations and hence it is expected to be more robust than alternative approaches. Indeed, the temperature ablation threshold can vary for different tissue types and hence the lesion size can be erroneously estimated even when considering an imaging approach that accurate maps the temperature distribution. Abrupt changes in the OA signal intensity can also enable identifying the onset of coagulation in ablation procedures based on a relatively large exposure time. Furthermore, the reported increase in optical attenuation in ablated tissues results in a reduced light fluence at deep locations.³⁰ Thereby, positive changes in the time derivative of OA signals are exclusively due to coagulation and can be detected at any point of the target tissue regardless of the light delivery method for OA excitation. The newly suggested method has been enabled by the unique OA capabilities for high-frame-rate imaging in three dimensions and for sensing chemical transformations taking place during coagulation. The fact that single wavelength excitation is sufficient for detecting such changes can also significantly reduce the cost of clinical embodiments. These features, along with the fact that non-ionizing radiation is employed, represent unparalleled advantages of OA with respect to other imaging modalities that can potentially be used for ablation monitoring. Multi-spectral OA imaging, based on tissue excitation at multiple optical wavelengths, can further provide additional information encoded both in the time and spectral dimensions.²¹ However, even though OA spectral changes have been detected in ablated tissues,[?] these may not be properly identified in regions affected by the wavelength dependence of optical attenuation and single-wavelength excitation may still represent the optimum approach for ablation monitoring. Overall, we expect that the methodology introduced in this work helps improving the outcome of tissue ablation methods routinely used in the clinics.

ACKNOWLEDGMENTS

The authors acknowledge the support by the German Research Foundation (DFG) and the Technical University of Munich within the funding program Open Access Publishing.

REFERENCES

- 1. Verma, A. & Natale, A. Circulation 121, p. 46–215, (2010).
- 2. Weininger, S., Pfefer, S. & Chang, I. A. *IEEE Symposium on Product Safety Engineering* **3-4**(2), p. 83–91, (2005).
- 3. Larin, K. V., Larina, I. V., Motamedi, M. & Esenaliev, R. O. SPIE Proc. 3916, p. 311–321, (2000).
- 4. Oyaga Landa, F. J. et. al. Noncontact monitoring of incision depth in laser surgery with air-coupled ultrasound transducers. *Optics letters.* **41**, p. 2704–2707, (2016).
- 5. Oyaga Landa, F. J. et. al. Noncontact monitoring of incision depth in laser surgery with air-coupled ultrasound transducers. *SPIE Digital Library*. **10064**, 100640H, (2017).
- 6. Teresawa, T., Balk, E. M. & Chung, M. Comparative Effectiveness Review 15, (2009).
- 7. Pai, M. et. al. World J Gastrointest Surg 7, p. 52–59, (2015).
- 8. Ahmed, M. et. al. Radiology **258**(2), p. 351–369, (2011).
- 9. Kaltman, J. R. et. al. J Cardiovascular Electrophysiology 19(2), p. 343–347, (2008).
- 10. January, C. T. et. al. Circulation 130, p. 2071–2104, (2014).
- 11. Xu, M. & Wang, L. et. al. *Physical Review E* **71**, p. 016706, (2005).

- 12. Rebling, J., Landa, F. J. O., Deán-Ben, X.L., Douplik, A. & Razansky, D. *Opt. Lett.* **130**, p. 2071–2104, (2014).
- 13. Rebling, J., Landa, F. J. O., Deán-Ben, X.L., Douplik, A. & Razansky, D. *SPIE Digital Library*. **10488**, p. 1048855, (2018).
- 14. Landa, F. J. O., Deán-Ben, X.L., Sroka, R. & Razansky, D. Scientific Reports 7, p. 9695, (2017).
- Oyaga Landa, F. J., Deán-Ben, X.L., Sroka, R. & Razansky, D. SPIE Digital Library 10494, p. 104940D, (2018).
- Oyaga Landa, F. J., Deán-Ben, X.L., Sroka, R. & Razansky, D. SPIE Digital Library 10415, p. 104150A, (2017).
- 17. Oyaga Landa, F. J., Ronda Penacoba, S., Deán-Ben, X.L., Montero de Espinosa, F. & Razansky, D. *Ultrasonics* **5860**, (2018).
- 18. Oyaga Landa, F. J., Ronda Penacoba, S., Deán-Ben, X.L., Montero de Espinosa, F. & Razansky, D. SPIE Digital Library 10494, 104945J, (2018).
- 19. Larina, I. V., Larin, K. V. & Esenaliev, R. O. Journal of Physics D: Applied Physics 38(15), p. 2633–2639, (2005).
- 20. Datta, N. R. et. al. *Cancer Treatments Reviews* **41**, p. 742–753, (2015).
- 21. Pang, G.A., Bay, E., Deán-Ben, X.L. & Razansky, D. *Journal of cardiovascular electrophysiology.* **26**(3), p. 339–345, (2015).
- 22. Fehm, T.F. et. al. J. Biophotonics. 9, p. 934–941, (2015).
- 23. Sapareto, S. A. & Dewey, W. C. Int. J. Radiat. Oncol. Biol. Phys. 10, p. 787–800, (1984).
- 24. Larin, K. V., Larina, I. V., Motamedi, M. & Esenaliev, R. O. SPIE Proc. 3916, p. 311–321, (2000).
- 25. Soroushian, B., Whelan, W. M. & Kolios, M. C. SPIE Proc. **75641N**, (2010).
- 26. ANSI: American National Standard for Safe Use of Lasers. American National Standard Institute, (2007).
- 27. Wang, L. V. & Wu, H. Biomedical optics: principles and imaging, (2010).
- 28. Cui, H. & Yang, X. Medical Physics 38(10), p. 5345, (2011).
- 29. Chin, L.C.L., Whelan, W. M., Sherar, M.D. & Vitkin, I.A. *Physics in Medicine & Biology* **46**(9), p. 2407–2420, (2001).
- 30. Meng, L. et. al. *Photoacoustics* **13**, p. 33–45, (2019).